ESKİŞEHİR TECHNICAL UNIVERSITY JOURNAL OF SCIENCE AND TECHNOLOGY
A- APPLIED SCIENCES AND ENGINEERING

2023, 24(4), pp. 309-323, DOI: 10.18038/estubtda.1330556

RESEARCH ARTICLE

THE EFFECT OF GRINDING ON OPTICAL BAND GAP AND URBACH ENERGY OF POLYPYRROLE/GRAPHENE COMPOSITES

Merve OKUTAN[1,*]

[1] Department of Chemical Engineering, Engineering Faculty, Hitit University, Çorum, Türkiye

ABSTRACT

The goal of this study is to better understand the effect of grinding on the Eg of polypyrrole (PPy)/commercial graphene nanoplatelets (xGnP) composites with varying amounts of xGnP. The Eg for direct transition as a function of the xGnP amount was calculated from the Tauc plot. While the average particle size of the composites decreased between 6% and 30%, there was a slight decrement in the Egs. These values changed between 4.02 to 3.87 eV with the increasing amount of xGnP before grinding, and they reached between 3.97 to 3.88 eV after grinding. Moreover, it was determined that the E_U was inversely proportional to Eg. These findings suggest that the PPy/xGnP composites could be suitable for several applications, such as photocatalytic and optoelectronic.

Keywords: Polypyrrole, Graphene, Tauc plot, Urbach energy, UV/Vis spectroscopy

1. INTRODUCTION

Polymeric semiconductors are frequently used in application areas such as transistors [1], electrochromic materials [2], photocatalysis [3], batteries [4], supercapacitors [5], corrosion [6], and biomedical devices [7] due to their superior properties. Among them, PPy is a well-known conjugated polymer that has been the focus of many studies due to its easy synthesis, good electrical properties, biocompatibility, low oxidation potential, chemical and environmental stability, large surface area, satisfying specific capacitance, processability, strong absorption spectral range and low cost [7-10]. However, the spherical polymer particles, which are easy to agglomerate, and their relatively low mechanical strength limit PPy usage for several applications. These problems can be overcome by preparing composites/nanocomposites of PPy with various carbon-derived materials [9,11]. Moreover, electrical and optical properties can be improved owing to the fast and easy electron/ion transfer that can be obtained with the contribution of a carbon network with high carrier transport mobility such as graphene [12]. Graphene modification of the PPy main chain is expected to control the interchain interaction and make this material, which acts as an electron donor/hole transporter under UV through the delocalized π-π* conjugated structure, more efficient for applications such as color change and photocatalysis by controlling the optical energy band gaps (Eg) [13]. It is important to monitor the electronic properties of PPy and its composites used in applications related to electronic and optical properties such as sensors, electronics, optics, and photovoltaic devices. Studies have been carried out to monitor the electronic properties with the change in optical band gap of these composites. Some of them in the literature investigating the Eg of PPy composites prepared with graphene derivatives are listed below. Bora and Dolui [9] studied a new procedure prepared for PPy/graphene via liquid-liquid interfacial polymerization and they remarked that the electrical conductivity and thermal stability of these materials were observably enhanced. The Eg of PPy and composites was determined as 2.33 eV and 2.10-1.82 eV according to increased graphene content, respectively. Liu et al. [13] reported that the graphitic carbon nitride and PPy composite, which was prepared via in-situ chemical polymerization of

*Corresponding Author: merveokutan@hitit.edu.tr
Received: 20.07.2023 Published: 27.12.2023

pyrrole, had narrowed Eg due to the PPy, and also the addition of reduced graphene oxide (rGO) into composite led to much lower Eg between 2.4 to 2.6 eV. Sadrolhosseini et al. [14] prepared the PPy/rGO nanocomposite with had particular thickness based on deposition time via electrochemical synthesis and determined the Eg between 3.580 to 3.853 eV with decreased deposition time. Noreen et al. [15] studied about photocatalytic and antibacterial properties of PPy/graphene composites that were synthesized via in-situ chemical oxidative polymerization. While the Eg of PPy was calculated as 2.38 eV, they reported that the Eg values of composites containing 10, 30, and 50% graphene were determined as 1.85 eV, 1.69 eV, and 1.63 eV, respectively. Ahmed and Hassan [16] investigated the optical and electrical properties of PPy/graphene composites prepared via in-situ polymerization. They stated that the Eg value of PPy by direct transition, which was 2.1 eV, decreased to 1.3 eV with the contribution of 5% graphene. In all of the limited number of studies mentioned above, $FeCl_3$ was used as the oxidant, regardless of the synthesis method. It is well known that the length of the conjugated chains obtained in the synthesis of conducting polymers has a direct effect on the physical properties of the polymer and the conjugation length is related to the type and ratio of the oxidant and dopant used [17]. In addition to $FeCl_3$, several oxidizing agents such as $FeClO_4$, $AgNO_3$, H_2O_2, and $(NH_4)_2S_2O_8$ have been used for the chemical oxidation of pyrrole [18]. When PPy was synthesized by chemical oxidative polymerization in acidic medium, it was reported that the electrical conductivity value was higher but the polymerization yield was lower than that of $(NH_4)_2S_2O_8$ when $FeCl_3$, which has low solubility in this medium, was used as oxidant [19]. Sood and co-workers used $FeCl_3$ and $(NH_4)_2S_2O_8$ as oxidants in the synthesis of PPy and compared the effect on thermal, electrical and morphological properties [18]. Dubey et al. investigated the characterization and morphological properties of PPy synthesized under ammonium per sulfate in the presence of anionic and cationic surfactants and their combinations for the energy storage capacity and its potential use in sensor applications of the prepared material [20]. Similarly, John and Jayalekshmi investigated the solubility, processability, electrical, optical and morphological properties of PPy synthesized with different dopants and ammonium per sulfate oxidant with a view to using the prepared material in potential technological applications [21]. Ravikiran et al. investigated the use of a physically prepared composite of PPy and reduced graphene oxide as a humidity sensor. Ammonium per sulfate was used as an oxidant in the synthesis of PPy [22]. Atta et al. investigated the use of PPy, synthesized in the presence of APS, and NiO conductive composites in optoelectronic devices [23]. In addition to these studies, the effect of grinding on the change in particle size was investigated to understand the optical properties of PPy and PPy/xGnP composites prepared using $(NH_4)_2S_2O_8$ as an oxidant in acidic medium. For this purpose, PPy and xGnP composites were synthesized via oxidative polymerization. Optical properties were investigated using ultraviolet-visible (UV-Vis) spectrophotometry. The Eg value was estimated via Tauc plot and Urbach tail energy (E_U) was calculated to determine defect levels based on xGnP amount for PPy based composites both before and after ball milling. In addition, while chemical and morphological properties of PPy and PPy/xGnP composites were investigated with Fourier transform infrared spectroscopy (FTIR), Raman spectroscopy, X-ray photoelectron spectroscopy (XPS), and transmission electron microscope (TEM)/scanning electron microscope (SEM) analysis; particle size of the composites was determined using a Zeta Sizer.

2. EXPERIMENTAL

2.1. Materials

Pyrrole (99.5%), hydrochloric acid (HCl, 37%) and xGnP nanoplatelets (grade C-750) were purchased from Sigma-Aldrich. Ammonium persulfate ($(NH_4)_2S_2O_8$, >98%) as an oxidizer agent was provided by Merck. Dimethyl sulfoxide (DMSO, >99%) was obtained by also Merck as a solvent for UV-Vis measurements. All chemicals were used as received.

2.2. Synthesis of PPy/xGnP Composites

PPy/xGnP composites were synthesized by oxidative polymerization of pyrrole monomer including xGnP at various loadings (1, 3, and 5 w/v) in the presence of HCl and $(NH_4)_2S_2O_8$. For this, 0.2 M pyrrole monomer and a proper amount of xGnP were mixed in 50 ml 1 M HCl. Then, 0.2 M $(NH_4)_2S_2O_8$ solution as oxidant, which was prepared in 1 M HCl, was added slowly to the monomer solution in an ice bath. The polymerization reaction was allowed at 0-5°C for 2 h under constant stirring. The obtained black product was filtrated and then washed several times with acid and ultra-pure water for purification. PPy/xGnP composite was dried at 80°C for 8 h [24]. In addition, PPy was synthesized without adding xGnP. To reveal the effect of grinding via ball milling on the Eg of composites, the prepared PPy/xGnP composites were ground in a Fritsch pulverisette 7 planetary ball mill at room temperature using a sintered alumina bowl and balls (balls to powder ratio was 10% w/w) at 500 rpm for 5 min through the forward and reverse. The samples were labelled as in Table 1.

Table 1. Abbreviations for PPy/xGnP composites according to ball milling.

	Abb.	Sample
Before ball milling (i:initial)	(PPy)i	Synthesized polypyrrole
	(PPy/xGnP1)i	Synthesized PPy/xGnP composite containing 1% (w/v) xGnP
	(PPy/xGnP3)i	Synthesized PPy/xGnP composite containing 3% (w/v) xGnP
	(PPy/xGnP5)i	Synthesized PPy/xGnP composite containing 5% (w/v) xGnP
After ball milling (bm: ground via ball milling)	(PPy)bm	Ball milled polypyrrole
	(PPy/xGnP1)bm	Ball milled PPy/xGnP composite containing 1% (w/v) xGnP
	(PPy/xGnP3)bm	Ball milled PPy/xGnP composite containing 3% (w/v) xGnP
	(PPy/xGnP5)bm	Ball milled PPy/xGnP composite containing 5% (w/v) xGnP

2.3. Characterization

The particle size distributions of the PPy, xGnP, and PPy/xGnP composites were determined using a ZetaSizer Nano ZSP laser particle analyser (Malvern). The FTIR of the PPy, xGnP, and PPy/xGnP composites was recorded by a Thermo Scientific Nicolet 6700 FTIR spectrometer equipped with an ATR (attenuated total reflectance) attachment in the wave number range from 600 to 4000 cm^{-1}. The Raman spectra of the PPy, xGnP, and PPy/xGnP composites were collected from a Renishaw Raman spectroscopy (532 nm). The optical properties of PPy, xGnP, and PPy/xGnP composites were studied using a UV-Vis spectrophotometer in the range of 200-800 nm by using Genesys 10S, Thermo USA. All samples were dispersed in DMSO at a concentration of 0.3 mg/mL using tip sonication for 15 min (Bandelin Sonopuls, type: UW 200, probe: TS113, ampl: 10%, pulse: 0.5s/1s). The TEM image of xGnP was taken from a JEOL JEM 1220 electron microscope and the morphological characterization of the (PPy/xGnP5)bm was performed with a field emission SEM (FESEM, Quanta 450 FEG model, 20-30 kV, FEI).

3. RESULTS AND DISCUSSION

3.1. ZetaSizer Analysis

Particle size distribution analysis by the intensity of PPy, xGnP, and PPy/xGnP composites before and after grinding with ball milling was performed with a ZetaSizer and the results are given in Figure 1. xGnP was a commercial product with a surface area 750 m^2 g^{-1}. Its average particle size was found to be around 168 nm (Figure 1a). While PPy showed an average particle size of 876 nm, the size of (PPy)bm was found 365 nm (Figures 1b and 1c). The average particle sizes of the composites containing 1, 3, and 5% of xGnP were determined to be 718, 853, and 1048 nm before ball milling (Figures 1d, 1e, and 1f). These values decreased to 674, 779, and 730 nm after grinding via ball milling (Figures 1g, 1h, and 1i), respectively. The results showed a slightly increasing trend in particle size with the ascending filler amount of composite. It is predicted that polymerization started after the adsorption of pyrrole to the electronegative oxygen atom on functional groups on the xGnP sheets [25]. Hence, PPy/xGnP composite particles were partially grown with the increment of the graphene amount in the composite due to the formation of PPy particles on the curved xGnP surface (see Figure 7b) during the synthesis [26].

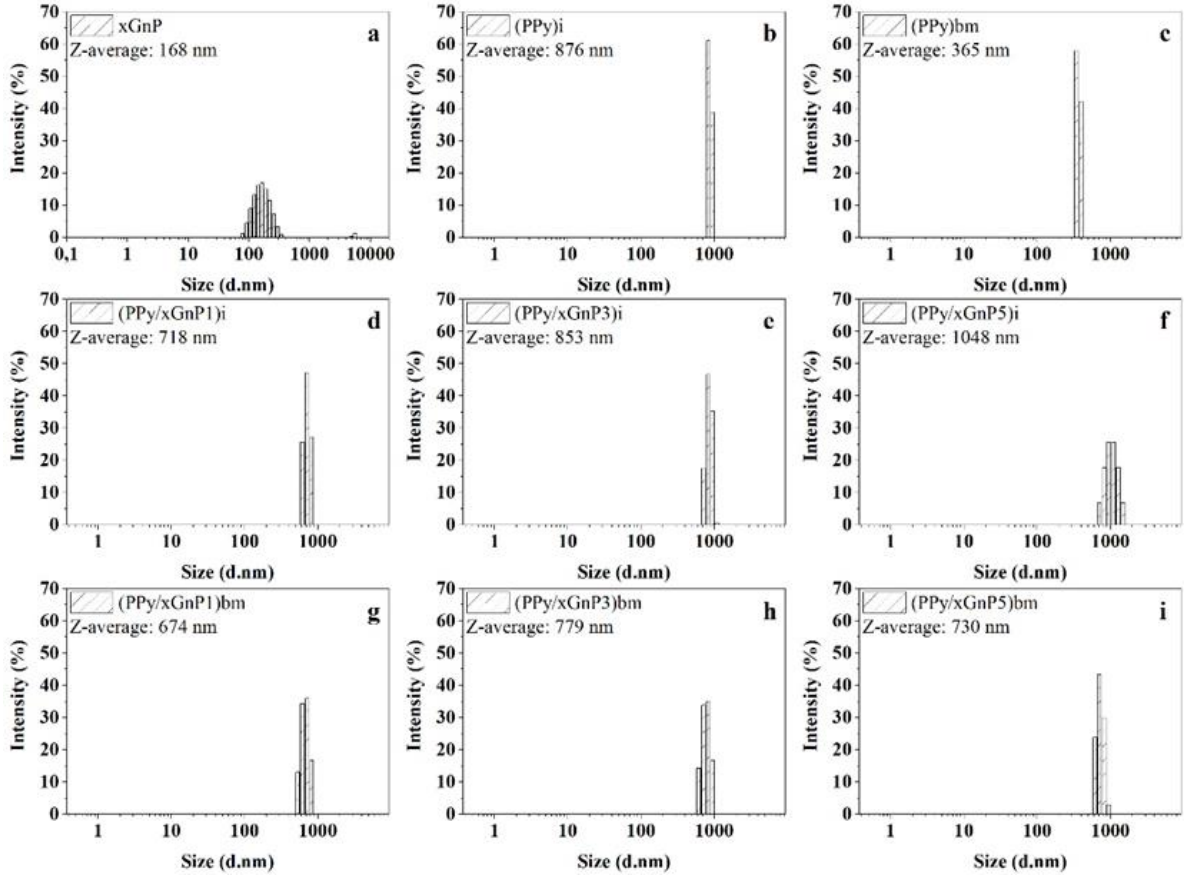

Figure 1. The particle size distribution by intensity of (a) xGnP; (b) (PPy)i, (c) (PPy)bm, (d) (PPy/xGnP1)i, (e) (PPy/xGnP3)i, (f) (PPy/xGnP5)i, (g) (PPy/xGnP1)bm, (h) (PPy/xGnP3)bm, and (i) (PPy/xGnP5)bm, respectively.

3.2. FTIR Analysis

The FTIR spectra of xGnP, PPy, and PPy/xGnP composites are given in Figure 2. The FTIR peaks of PPy at 1546 cm^{-1}, 1461 cm^{-1}, and 3433 cm^{-1} were attributed to the C-C, C-N, and N-H stretching vibrations of the ring structure in pyrrole. The peaks at 1690 cm^{-1}, 1169 cm^{-1}, and 1027 cm^{-1} can be assigned to C=N bonds, C-N in-plane vibration, and C-H band in-plane vibration for PPy, respectively. The peaks at about 2920 cm^{-1} and 2850 cm^{-1} in all spectra were associated with asymmetrical and symmetrical ring vibrations of CH_2. The carbonyl peak (-COOH) at 1723 cm^{-1}, the C-O stretching vibration at 1058 cm^{-1} and the hydroxyl group (-OH) at 3467 cm^{-1} of xGnP showed the oxygen-containing functional groups on the graphene surface. Also for xGnP, a strong band of the stretching and deformation vibrations of CH_2 appeared at about 2332 cm^{-1}. The presence of characteristic peaks of PPy in composites spectra confirmed the existence of PPy in the composites. The shift of the C=O peak to nearly 1760 cm^{-1} was probably related to the π-π interaction of the aromatic PPy ring with oxygenated functional groups on xGnP. In short, these changes proved that the combination of graphene in the PPy matrix and the composites were successfully synthesized [9,25,27-30].

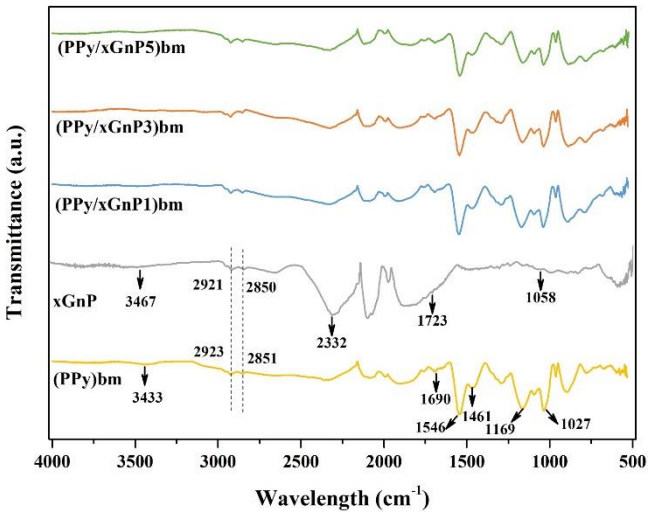

Figure 2. FTIR spectra of xGnP, (PPy)bm, (PPy/xGnP1)bm, (PPy/xGnP3)bm, and (PPy/xGnP5)bm.

3.3. Raman Analysis

The Raman spectra of xGnP, PPy, and PPy/xGnP composites are given in Figure 3. The xGnP spectrum in Figure 3a displayed three distinctive Raman bands at about 1323 cm^{-1}, 1576 cm^{-1}, and 2636 cm^{-1}, which were attributed to the D, G, and 2D bands, respectively. The characteristic Raman bands at about 1355 cm^{-1} and 1570 cm^{-1} corresponded with the C-N ring stretching and C=C backbone stretching for PPy (Figure 3a), which these Raman bands were in approximately the same position with D and G bands of graphene. The almost same bands were seen in Raman spectra of PPy/xGnP composites (Figure 3a). However, in the Raman spectra of composites, both D and G bands were shifted between 1330-1340 cm^{-1} and 1550-1570 cm^{-1}, which indicated the π-π interaction between PPy and xGnP. Furthermore, since the double bonds between the carbon atoms and other conjugated bonds lead to increase in the Raman intensities, the Raman intensities of polymer and polymer composites were higher than that of the commercial graphene as seen in Figure 3a [31-34].

In Raman spectroscopy, the D band indicates sp^3 hybridization and the amount of structural defects and edges, while the G band indicates sp^2 hybridization and a more ordered structure. In other words, the higher intensity of the D band indicates that the graphite network of the material has more defects. In addition, a more distinct G band means that the material has a more crystalline structure. The information about the structural defect can be obtained by proportioning the intensities of the D and G bands, as having similar intensities indicates the highly defective structure [31,35,36]. As seen in Figure 3b, I_D/I_G ratios for each sample were calculated by reading and proportioning the Raman band intensities at the wavelengths specified for the D and G bands in the spectrum. Although the prepared composites had a slightly ordered structure compared to xGnP, I_D/I_G ratios were almost the same. While various functionalization processes are expected to increase the defect ratio in the structure, it is predicted that there was no significant change in the size of the average sp^2 domains because of the PPy/xGnP interaction [37]. As a second opinion, it can be evaluated that the prepared composites were quite defective compared to xGnP. Because this ratio can be lower than graphene in highly defective materials where the distance between defects is less than two nm [38].

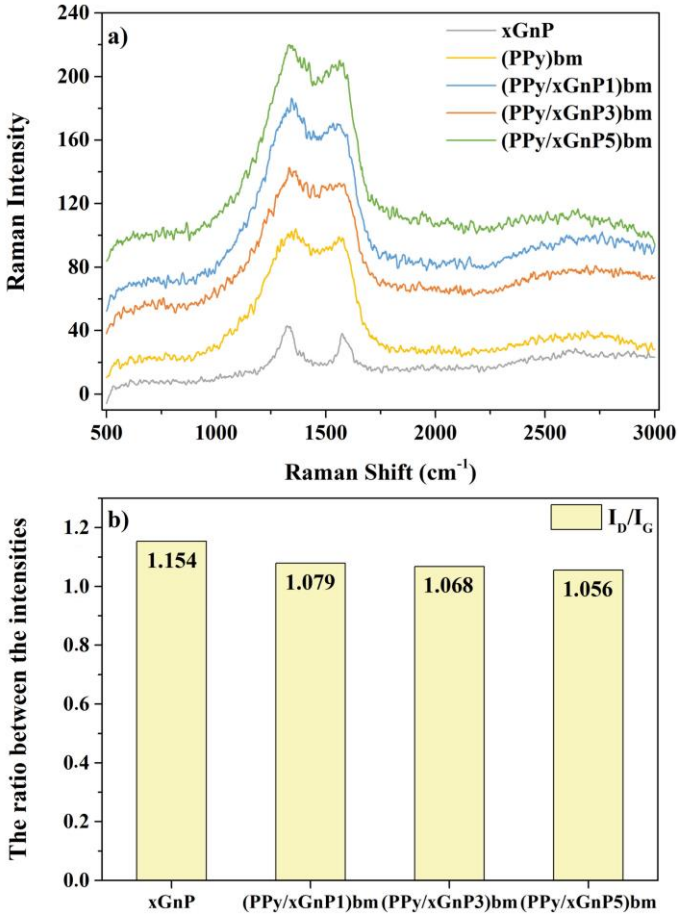

Figure 3. (a) Raman spectra and (b) I_D/I_G ratios of xGnP, (PPy)bm, (PPy/xGnP1)bm, (PPy/xGnP3)bm, and (PPy/xGnP5)bm.

3.4. XPS Analysis

XPS analysis was carried out to examine the chemical state and composition of PPy, xGnP, and PPy/xGnP composites and the spectra are shown in Figure 4. As is seen from Figure 4, the xGnP had

C1s core level peaks at 284.4 eV that could be attributed to the C-C bond, and the peak at ~288.8 eV was related to the C=O bond [39]. The N1s core level peak was absent in the xGnP, while it was seen in the PPy samples spectra, which is related to the polymerization of pyrrole [40]. In addition, Figure 4 is depicted the presence of characteristic O1s (~531 eV), C1s (~ 284 eV), N1s (~399 eV), and S2p (~168 eV) peaks both for the PPy and its composites with xGnP. The S2p core level peak was generated from $(NH_4)_2S_2O_8$, which was used as an oxidant for the polymerization of PPy. The change in the binding energies of PPy to higher energy levels for composites (O1s (~532 eV), C1s (~ 285 eV), N1s (~400 eV)) was related to the π-π interaction between the PPy and xGnP, which is in good agreement with the FTIR and Raman results. The core level peak of C-N at ~285 eV was also confirmed to be the PPy moiety in the xGnP structure. The N1s core level peaks at ~399 and ~400 eV were attributed to the -N-H group in the pyrrole ring and positively charged N of polaron ($-N-H^+$). The rising energy level from 399 to 400 eV was associated with the migration of the neutral secondary amine, which also indicated a strong π-π interaction [39,41,42]. Furthermore, the Cl2p peak (~198 eV) was observed in all PPy samples due to the HCl as the dopant [43]. This confirmed the successful preparation of PPy/xGnP composites.

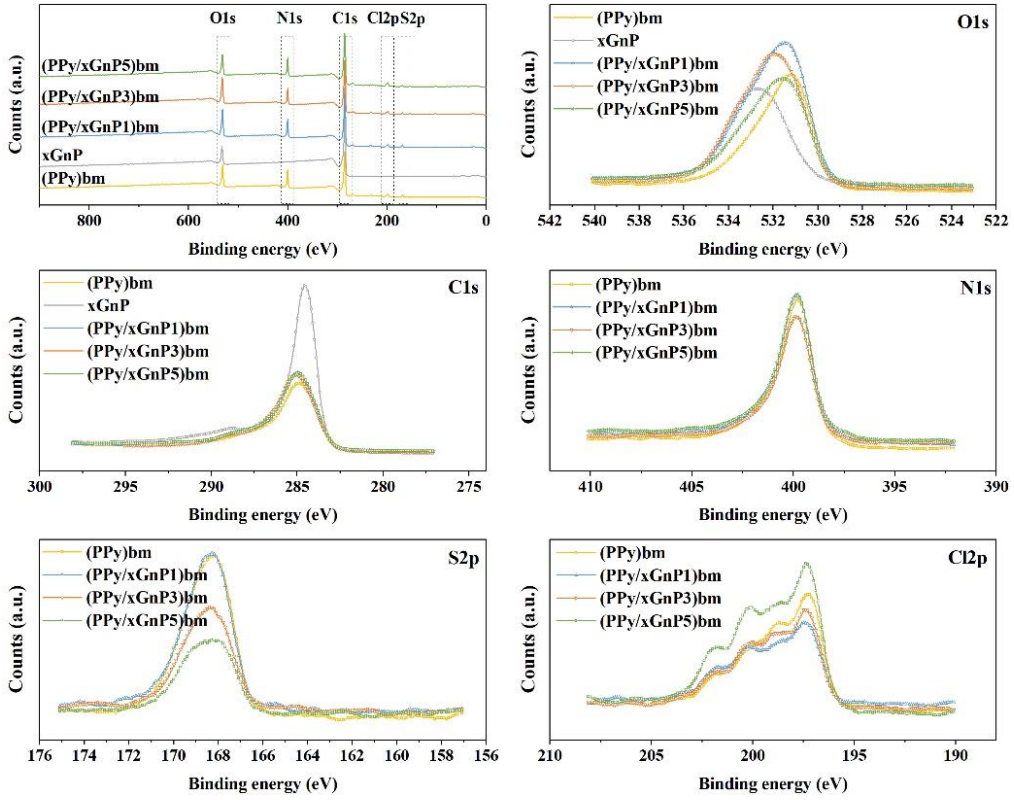

Figure 4. General and elemental (O1s, C1s, N1s, S2p, Cl2p) XPS spectra of the xGnP, (PPy)bm, (PPy/xGnP1)bm, (PPy/xGnP3)bm, and (PPy/xGnP5)bm.

3.5. UV-Vis Analysis

The UV-Vis absorption spectra of xGnP, PPy, and PPy/xGnP composites recorded in DMSO are shown in Figures 5a and 5c. xGnP showed a distinctive peak at 279 nm which, is dedicated to the π-π* transition of the C=C bonds. For the PPy and PPy/xGnP composites, the spectra showed a characteristic band at around 275-281 nm due to the π-π* interactions for C=C group. In addition to this peak, the spectra of synthesized composites displayed a broad absorption band between 350-400 nm related to the π-π* transitions for the C=N group. After the ball milling, the peak that related to the sp^2 C=C bands of the

composites was slightly shifted. It was thought that this behavior could be explained by the restoration of π conjugation regions due to the change in particle size. In addition, the increase in the xGnP ratio in the composite caused an increase in the absorbance value. Similar results were observed for the UV-Vis spectra in the literature [44-48].

The Eg (eV) of xGnP, PPy, and PPy/xGnP composites was obtained with UV-Vis absorbance spectrum and the Eg values were calculated using Tauc plot as follows (Equation 1).

$$(\alpha h\nu)^{1/m} = B(h\nu - E_g) \tag{1}$$

$$\alpha(\lambda) = \left(\frac{2.303}{d}\right) A(\lambda) \tag{2}$$

where α (cm^{-1}) is the absorption coefficient which is given in Equation 2, d is sample width (cm), A is absorbance from UV-Vis analysis, h is the Planck's constant ($4.14x10^{-15}$ eVs), ν is the frequency (s^{-1}), B is a comparative constant, and m is a constant related to the electronic transition type which is equal to 1/2 for direct transition. The experimental method should be used to determine the most appropriate value of m. According to Equation 1, the Eg value should be directly proportional to $(\alpha h\nu)^{1/m}$. For this reason, these linear parts of the irregular graph drawn by calculating the $(\alpha h\nu)^{1/m}$ and hν values are taken into account. The Eg value is determined as the intersection of the hν axis by extrapolation from the linear part [49-51].

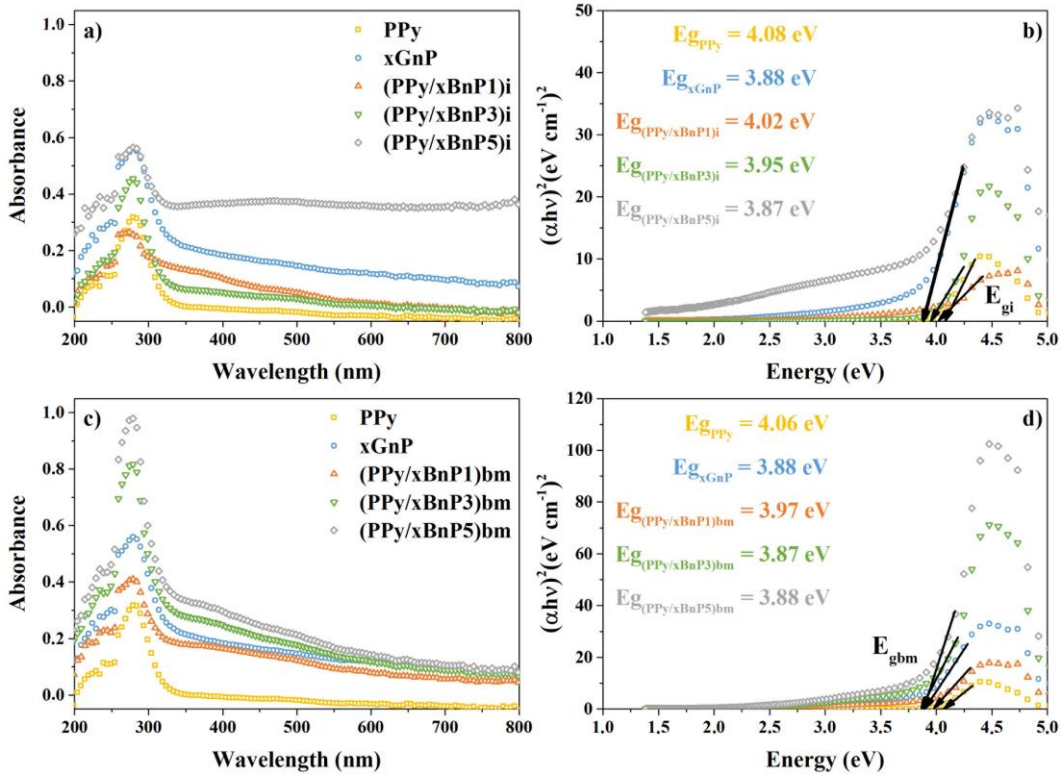

Figure 5. UV-Vis absorption spectra and Tauc plot for direct transition of xGnP, PPy, and PPy/xGnP composites (a,b) before and (c,d) after ball milling, respectively.

The Tauc plot was used to estimate the Eg for direct transition of xGnP, PPy, and PPy/xGnP composites before and after ball milling are given in Figures 5b and 5d. Based on the Tauc plot, the calculated Eg of xGnP was estimated to be ~3.88 eV for direct band gap transition. As can be seen from the Figures 5b and 5d, the Eg values of PPy decreased as the amount of xGnP in the composite increased, both before and after ball milling. These results showed that the number of electrons/holes in the valence and conduction bands changed due to the presence of new charge transfer complexes formed between PPy and xGnP and the disorder created in a polymer matrix [48,52,53]. In addition, there was a slight decrease in Eg_{bm} values compared to Eg_i.

In semiconductors, if sub-bands form between the conduction and valence bands or there are defects, a defect tail is formed, which is known as the Urbach tail, under the conduction band and above the valance band. In this region, to estimate the defect level and the localized states in the forbidden band gap, the E_U can be calculated from Equation 3.

$$\ln(\alpha) = ln(\alpha_0) + (\frac{h\nu}{E_U}) \tag{3}$$

where α_0 is a constant, hν is the energy, and the E_U is Urbach energy [48,54]. For the determination of the E_U, the first ln(α)-hν graph is drawn. Then, in this region (below the Eg value), the E_U value can be calculated in the slope of the linear graph obtained from the curve of the logarithm of the absorption coefficient versus the energy. The E_U results calculated for PPy samples were given in Table 2 and the linear part of the graph of ln(α) versus hν was given in Figure 6.

Table 2. E_U of xGnP, PPy, and PPy/xGnP composites.

Samples	E_U (eV)
xGnP	2.8234
PPy	0.1392
(PPy/xGnP1)i	0.9238
(PPy/xGnP3)i	1.2741
(PPy/xGnP5)i	9.8649
(PPy/xGnP1)bm	2.1852
(PPy/xGnP3)bm	2.3085
(PPy/xGnP5)bm	2.3935

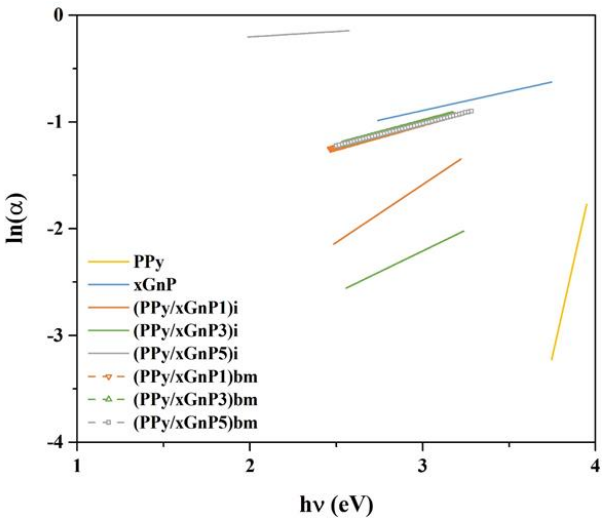

Figure 6. ln(α) of xGnP, PPy, and PPy/xGnP composites versus hυ.

It was determined that the E_U value of PPy was increased with the increase of xGnP in the composite both before and after ball milling. These results were inversely proportional to Eg change. Furthermore, it displayed that the xGnP led to a lower energy transition in the composites and the degree of disordering in the polymeric structure progressed due to the increasing localized states in the forbidden band gaps in the PPy structure. The results obtained are in agreement with the literature [16,48,52,53].

3.6. Surface Morphology Analysis

The structural morphology of xGnP and (PPy/xGnP5)bm composite was investigated by TEM and SEM analysis. From the TEM image of xGnP, which is given in Figure 7a, partially wrinkled and transparent graphene sheets could be clearly seen. This wrinkled sheet like morphology, seen in the literature for graphene, has been interpreted as a reduction in the angular tension between carbon bonds due to changes between sp^2 and sp^3 hybridized carbon atoms and the atomic arrangement becoming more stable by taking on a wrinkled aspect [55,56]. The SEM image for the (PPy/xGnP5)bm is given in Figure 7b. The formation of the composite can be described as the uniform absorption of the pyrrole on the xGnP surface through non-covalent interaction and polymerization and coating of PPy on the xGnP surface via in-situ polymerization [40]. From the figure, it can be seen that the almost uniform PPy particles of granular or spherical shape were embedded on the graphene sheet. Consequently, this image indicated that the pyrrole polymerization took place on the graphene sheets, and PPy was successfully anchored on the xGnP surface [9,14,57].

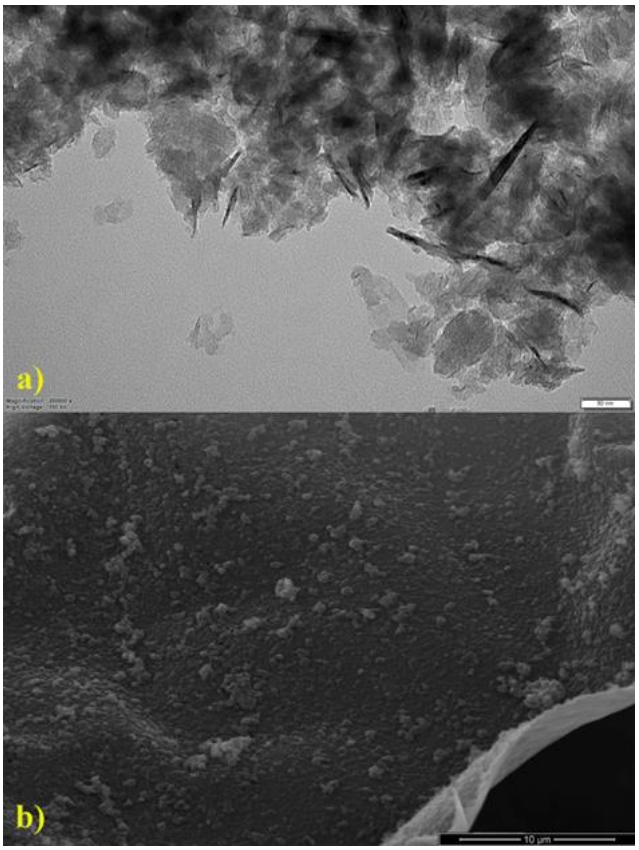

Figure 7. (a) TEM image of xGnP (scale bar 50 nm) and (b) SEM image of (PPy/xGnP5)bm (mag. 10,000 x, scale bar 10 μm).

4. CONCLUSION

The present study describes the synthesis of PPy and PPy/xGnP composites via oxidative polymerization of pyrrole in the presence of $(NH_4)_2S_2O_8$ as an oxidant. The effect of the grinding via ball milling on the Eg and structural defects of these materials was then investigated. The Eg of the samples was calculated using UV-Vis absorption spectrophotometry. The FTIR, Raman, and XPS analysis revealed the change of the functional groups on PPy and xGnP after the composite preparation. The UV-Vis analysis confirmed the decrease in Eg calculated from the Tauc plot for the direct transition of the composites after ball milling. The decrease in band gap energy with both ball milling and increasing graphene content is attributed to the change in defect levels of the composite structure. Furthermore, the E_U value changed from 0.1392 eV for PPy to 2.3935 eV for (PPy/xGnP5)bm indicating that the defect in the polymer structure increased with the addition of xGnP to the composite. These results indicate that the optical properties improved slightly after grinding. It is expected that these findings will be helpful for several applications such as electronic, optic, and sensing.

CONFLICT OF INTEREST

The author stated that there are no conflicts of interest regarding the publication of this article.

REFERENCES

[1] Wang Y, Qing X, Zhou Q, Zhang Y, Liu Q, Liu K, Wang W, Li M, Lu Z, Chen Y et al. The woven fiber organic electrochemical transistors based on polypyrrole nanowires/reduced graphene oxide composites for glucose sensing. Biosens Bioelectron. 2017; 95: 138-145.

[2] Bezgin Carbas B, Ergin NM, Yildiz HB, Kivrak A, Demet AE. Electrochromic properties of a polydithienylpyrrole derivative with n-phenyl pyrrole subunit. Mater Chem Phys. 2023; 293: 126916.

[3] Ahmad N, Sultana S, Sabir S, Khan MZ. Exploring the visible light driven photocatalysis by reduced graphene oxide supported PPy/CdS nanocomposites for the degradation of organic pollutants. J Photochem Photobiol A Chem. 2020; 386: 112129.

[4] Folorunso O, Hamam Y, Sadiku R, Ray SS, Adekoya GJ. Investigation of graphene loaded polypyrrole for lithium-ion battery. Mater Today Proc. 2021; 38: 635-638.

[5] Gupta A, Sardana S, Dahiya S, Punia R, Maan AS., Singh K, Tripathi R, Ohlan A. Binder-free polypyrrole/fluorinated graphene nanocomposite hydrogel as a novel electrode material for highly efficient supercapacitors. Appl Surf Sci Adv. 2022; 11: 100297.

[6] Qiu S, Li W, Zheng W, Zhao H, Wang L. Synergistic effect of polypyrrole-intercalated graphene for enhanced corrosion protection of aqueous coating in 3.5% NaCl solution. ACS Appl Mater Interfaces. 2017; 9: 34294-34304.

[7] Zare EN, Agarwal T, Zarepour A, Pinelli F, Zarrabi A, Rossi F, Ashrafizadeh M, Maleki A, Shahbazi MA, Maiti TK et al. Electroconductive multi-functional polypyrrole composites for biomedical applications. Appl Mater Today. 2021; 24: 101117.

[8] Hao L, Yu D. Progress of conductive polypyrrole nanocomposites. Synth Met. 2022; 290: 117138.

[9] Bora C, Dolui SK. Interfacial synthesis of polypyrrole/graphene composites and investigation of their optical, electrical and electrochemical properties. Polym Int. 2014; 63: 1439-1446.

[10] Krishnaswamy S, Ragupathi V, Raman S, Panigrahi P, Nagarajan GS. Optical properties of p-type polypyrrole thin film synthesized by pulse laser deposition technique: Hole transport layer in electroluminescence devices. Optik (Stuttg). 2019; 194: 163034.

[11] Wilczewska P, Breczko J, Bobrowska DM, Wysocka-Żołopa M, Goclon J, Basa A, Winkler K. Enhancement of polypyrrole electrochemical performance with graphene quantum dots in polypyrrole nanoparticle/graphene quantum dot composites. J Electroanal Chem. 2022; 923: 116767.

[12] Velasco-Soto MA, Pérez-García SA, Alvarez-Quintana J, Cao Y, Nyborg L, Licea-Jiménez L. Selective band gap manipulation of graphene oxide by its reduction with mild reagents. Carbon N Y. 2015; 93: 967-973.

[13] Liu S, Jiang X, Waterhouse GIN, Zhang ZM, Yu L. Protonated graphitic carbon nitride/polypyrrole/reduced graphene oxide composites as efficient visible light driven photocatalysts for dye degradation and E. coli disinfection. J Alloys Compd. 2021; 873: 159750.

[14] Sadrolhosseini AR, Abdul Rashid S, Noor ASM, Kharazmi A, Lim HN, Mahdi MA. Optical band gap and thermal diffusivity of polypyrrole-nanoparticles decorated reduced graphene oxide nanocomposite layer. J Nanomater. 2016; 2016(Article ID 1949042): 1-8.

[15] Noreen H, Iqbal J, Arshad A, Faryal R, Ata-ur-Rahman, Khattak R. Sunlight induced catalytic degradation of bromophenol blue and antibacterial performance of graphene nanoplatelets/polypyrrole nanocomposites. J Solid State Chem. 2019; 275: 141-148.

[16] Ahmed, F.M., Hassan, S.M. Optical and A.C. electrical properties for polypyrrole and polypyrrole/graphene (ppy/gn) nanocomposites. Iraqi J Phys. 2021; 19: 72-78.

[17] Dey S, Kumar KA. Morphological and optical properties of polypyrrole nanoparticles synthesized by variation of monomer to oxidant ratio. Mater Today Proc. 2019; 18: 1072-1076.

[18] Sood Y, Mudila H, Katoch A, Lokhande PE, Kumar D, Sharma A, Kumar A. Eminence of oxidants on structural–electrical property of polypyrrole. J Mater Sci Mater Electron. 2023; 34: 1401.

[19] Li XG, Li A, Huang MR, Liao Y, Lu YG. Efficient and Scalable Synthesis of Pure Polypyrrole Nanoparticles Applicable for Advanced Nanocomposites and Carbon Nanoparticles. J Phys Chem C. 2010; 114: 19244-19255.

[20] Dubey N. A study on surfactant modified polypyrrole nanostructures and its applications in supercapacitors. Int J Polym Anal Charact. 2023; 28: 625-646.

[21] John J, Jayalekshmi S. Polypyrrole with appreciable solubility, crystalline order and electrical conductivity synthesized using various dopants appropriate for device applications. Polym Bull. 2023; 80: 6099-6116.

[22] Ravikiran YT, Chethan B, Prasad V, Raj Prakash HG, Prashantkumar M, Tiwari SK, Thomas S. Polypyrrole/reduced graphene oxide composite as a low-cost novel sensing material for fast-response humidity sensor. Mater Chem Phys. 2023; 303: 127800.

[23] Atta A, Abdeltwab E, Negm H, Al-Harbi N, Rabia M, Abdelhamied MM. Characterization and linear/non-linear optical properties of polypyrrole/NiO for optoelectronic devices. Inorg Chem Commun. 2023; 152: 110726.

[24] Deligöz H, Tieke B. Conducting composites of polyurethane resin and polypyrrole: solvent-free preparation, electrical, and mechanical properties. Macromol Mater Eng. 2006; 291: 793-801.

[25] Manivel P, Kanagaraj S, Balamurugan A, Ponpandian N, Mangalaraj D, Viswanathan C. Rheological behavior-electrical and thermal properties of polypyrrole/graphene oxide nanocomposites. J Appl Polym Sci. 2014; 131: 40642(1-10).

[26] Li S, Wu D, Cheng C, Wang J, Zhang F, Su Y, Feng X. Polyaniline-coupled multifunctional 2D metal oxide/hydroxide graphene nanohybrids. Angew Chemie Int. 2013; 52: 12105-12109.

[27] Bose S, Kim NH, Kuila T, Lau K, Lee JH. Electrochemical performance of a graphene-polypyrrole nanocomposite as a supercapacitor electrode. Nanotechnology. 2011; 22: 295202.

[28] Fan X, Yang Z, He N. Hierarchical nanostructured polypyrrole/graphene composites as supercapacitor electrode. RSC Adv. 2015; 5: 15096-15102.

[29] Basavaraja C, Kim WJ, Thinh PX, Huh DS. Electrical conductivity studies on water-soluble polypyrrole-graphene oxide composites. Polym Compos. 2011; 32: 2076-2083.

[30] lam SN, Kumar L, Sharma N. Development of Cu-exfoliated graphite nanoplatelets (xGnP) metal matrix composite by powder metallurgy route. Graphene. 2015; 04: 91-111.

[31] Bora C, Dolui SK. Fabrication of polypyrrole/graphene oxide nanocomposites by liquid/liquid interfacial polymerization and evaluation of their optical, electrical and electrochemical properties. Polymer (Guildf). 2012; 53: 923-932.

[32] Alves APP, Koizumi R, Samanta A, Machado LD, Singh AK, Galvao DS, Silva GG, Tiwary CS, Ajayan PM. One-step electrodeposited 3D-ternary composite of zirconia nanoparticles, rGO and polypyrrole with enhanced supercapacitor performance. Nano Energy. 2017; 31: 225-232.

[33] Liu A, Li C, Bai H, Shi G. Electrochemical deposition of polypyrrole/sulfonated graphene composite films. J Phys Chem C. 2010; 114: 22783-22789.

[34] Rosas-Laverde NM, Pruna AI, Busquets-Mataix D. Graphene oxide-polypyrrole coating for functional ceramics. Nanomaterials. 2020; 10: 1188.

[35] Ferrari AC. Raman spectroscopy of graphene and graphite: disorder, electron-phonon coupling, doping and nonadiabatic effects. Solid State Commun. 2010; 143: 47-57.

[36] Okutan M. Electrochemical determination of ascorbic acid with thermally reduced graphene oxide. Gazi Üniversitesi Mühendislik-Mimarlık Fakültesi Derg. 2020; 35: 1589-1601.

[37] Khademeh Molavi F, Ghasemi I, Messori M, Esfandeh M. Nanocomposites based on poly(L-lactide)/poly(ε-caprolactone) blends with triple-shape memory behavior: effect of the incorporation of graphene nanoplatelets (GNps). Compos Sci Technol. 2017; 151: 219-227.

[38] Kovtun A, Treossi E, Mirotta N, Scidà A, Liscio A, Christian M, Valorosi F, Boschi A, Young RJ, Galiotis C et al. Benchmarking of graphene-based materials: real commercial products versus ideal graphene. 2D Mater. 2019; 6: 25006.

[39] Purkait T, Singh G, Kamboj N, Das M, Dey RS. All-porous heterostructure of reduced graphene oxide–polypyrrole–nanoporous gold for a planar flexible supercapacitor showing outstanding volumetric capacitance and energy density. J Mater Chem A. 2018; 6: 22858-22869.

[40] Tran XT, Park SS, Song S, Haider MS, Imran SM, Hussain M, Kim HT. Electroconductive performance of polypyrrole/reduced graphene oxide/carbon nanotube composites synthesized via in situ oxidative polymerization. J Mater Sci. 2019; 54: 3156-3173.

[41] Šetka M, Calavia R, Vojkůvka L, Llobet E, Drbohlavová J, Vallejos S. Raman and XPS studies of ammonia sensitive polypyrrole nanorods and nanoparticles. Sci Rep, 2019; 9: 8465.

[42] Wang J, Fu D, Ren B, Yu P, Zhang X, Zhang W, Kan K. Design and fabrication of polypyrrole/expanded graphite 3D interlayer nanohybrids towards high capacitive performance. RSC Adv. 2019; 9: 23109-23118.

[43] Cao J, Wang Y, Chen J, Li X, Walsh FC, Ouyang JH, Jia D, Zhou Y. Three-dimensional graphene oxide/polypyrrole composite electrodes fabricated by one-step electrodeposition for high performance supercapacitors. J Mater Chem A. 2015; 3: 14445-14457.

[44] Johra FT, Lee JW, Jung WG. Facile and safe graphene preparation on solution based platform. J Ind Eng Chem. 2014; 20: 2883-2887.

[45] Chaudhary K, Aadil M, Zulfiqar S, Ullah S, Haider S, Agboola PO, Warsi MF, Shakir I. Graphene oxide and reduced graphene oxide supported ZnO nanochips for removal of basic dyes from the industrial effluents. fullerenes, Nanotub Carbon Nanostructures. 2021; 29: 915-928.

[46] Yalçınkaya S, Çakmak D. Electrochemical synthesis of poly(pyrrole-co-[Cu(salabza)]): its electrocatalytic activity towards the oxidation of catechol. Hacettepe J Biol Chem. 2016; 44: 425-434.

[47] Nayak J, Mahadeva SK, Kim J. Characteristics of flexible electrode made on cellulose by soluble polypyrrole coating. Proc Inst Mech Eng Part C J Mech Eng Sci. 2012; 226: 2605-2609.

[48] Al-Harbi LM, Alsulami QA, Farea MO, Rajeh A. Tuning optical, dielectric, and electrical properties of polyethylene oxide/carboxymethyl cellulose doped with mixed metal oxide nanoparticles for flexible electronic devices. J Mol Struct. 2023; 1272: 134244.

[49] Johannes AZ, Pingak RK, Bukit M. Tauc plot software: calculating energy gap values of organic materials based on ultraviolet-visible absorbance spectrum. IOP Conf Ser Mater Sci Eng. 2020; 823: 012030.

[50] Tauc J. Optical properties and electronic structure of amorphous Ge and Si. Mater Res Bull. 1968; 3: 37-46.

[51] Guimarães ML, da Silva FAG, da Costa MM, de Oliveira HP. Coating of conducting polymer-silver nanoparticles for antibacterial protection of nile tilapia skin xenografts. Synth Met. 2022; 287: 117055.

[52] Alzahrani HS, Al-Sulami AI, Alsulami QA, Rajeh A. A systematic study of structural, conductivity, linear, and nonlinear optical properties of PEO/PVA-MWCNTs/ZnO nanocomposites films for optoelectronic applications. Opt Mater (Amst). 2022; 133: 112900.

[53] Ali HE, Khairy Y, Sayed MA, Algarni H, Shkir M, Maged FA. A. tailoring the linear/nonlinear optical and visible shielding performance of PVP/PVOH incorporated with NiO nanoparticles for optical devices. Optik (Stuttg). 2022; 251: 168373.

[54] Sharma N, Prabakar K, Ilango S, Dash S, Tyagi AK. Optical band-gap and associated Urbach energy tails in defected ain thin films grown by ion beam sputter deposition: Effect of Assisted Ion Energy. Adv Mater Proc. 2021; 2: 342-346.

[55] Boran F, Çetinkaya Gürer S. The effect of starting material types on the structure of graphene oxide and graphene. Turkish J Chem. 2019; 43: 1322-1335.

[56] Oliveira AEF, Braga GB, Tarley CRT, Pereira AC. Thermally reduced graphene oxide: synthesis, studies and characterization. J Mater Sci. 2018; 53: 12005-12015.

[57] Boran F, Çetinkaya S, Anaklı D, Karakışla M, Saçak M. Synthesis and characterization of Poly (o-toluidine)/Na-Feldspar conductive composites with improved electrical conductivity. Mühendislik Derg. 2017; 8: 901-910.